Graphene Oxide Based Biosensing Platform

By

Arash Darbandi

B.S., University of Illinois at Chicago, 2014

THESIS

Submitted as partial fulfillment of the requirements

for the degree of Master of Science in Bioengineering

in the Graduate College of the

University of Illinois at Chicago, 2017

Chicago, Illinois

Defense Committee:

Dr. Michael Stroscio, Chair and Advisor

Dr. Tolou Shokuhfar

Dr. Richard L Magin

Acknowledgements

I would like to thank my thesis advisor Dr. Michael Stroscio for providing motivation, experience, knowledge, mentoring, and funding given to me during the work presented in this thesis. I would additionally like to thank him for introducing me to the field of nanotechnology and opening my curiosity about this fascinating area of study. I would also like to thank my thesis committee -- Dr. Tolou Shokuhfar and Dr. Richard L. Magin -- for providing support and guidance in accomplishing my professional goals.

I also would like to thank my fellow graduate research assistants Debopam Datta and Shreya Ghosh and undergraduates Gary Ling and Krunal Patel for creating a great working environment and aiding throughout various projects we worked on in lab.

Lastly, but certainly not least, I would like to thank my parents Dr. Saeed Darbandi and Dr. Susan Yazdanmehr and my brothers – Azad and Aria – for providing support throughout my professional and non-professional life.

This work was supported in part by Army Research Office (ARO) through the MURI Grant No. W911NF-11-1-0024.

Table of Contents

List of Figures and Tables

List of Abbreviations

DNA	Deoxyribonucleic Acid
SELEX	Systematic Evolution of Ligands by Exponential Enrichment
ssDNA	Single stranded DNA
A	Adenine
T	Thymine
G	Guanine
C	Cytosine
QD	Semiconductor Quantum Dots
AuNP	Gold Nanoparticles
GO	Graphene Oxide
FRET	Fluorescence Resonant Energy Transfer
NSET	Nanometal Surface Energy Transfer
AAS	Atomic Absorption Spectroscopy
ICP-ES	Inductively Coupled Plasma Emission Spectroscopy
EDTA	Ethylenediaminetetraacetic acid
TCEP	Tris(2-carboxyethyl) phosphine hydrochloride
EDC	1-Ethyl-3-(3-dimethylaminopropyl) carbodiimide
Sulfo-NHS	N-hydroxysulfosuccinimide
MWCO	Molecular Weight Cut Off
PL	Photoluminescence
QE	Quenching Efficiency
LOD	Limit of Detection
DOX	doxorubicin
CPT	Camptothecin

Summary

The intersection of nanomaterials with biomolecules has been an area of much recent research interest. The inherently small sizes of nanomaterials such as semiconductor quantum dots and gold nanoparticles allow for unique optical and electronic properties that can be used in the field of medicine. One of the applications has been in the field of sensor science. Combing the optical and size properties of these materials has allowed for biotagging of cells and cellular components. Additionally, their small nature allows for the design of biosensors that detect desired analytes at a small scale. In this research, a novel "turn off" biosensor was designed for mercury detection.

A mercury sensitivity molecular beacon was fabricated using a quantum dot, gold nanoparticle, mercury target aptamer, and a DNA linker strand. When excited by an incident light, the quantum dot releases photons at 655 nm wavelength. The photons provide an optical signal that was detected using photoluminescence spectroscopy. The fluorescent indicator was then bioconjugated to a mercury sensitivity aptamer linked to a gold nanoparticle. Mercury ions bind to the thymine bases, causing the aptamer to undergo a conformational change to form a hairpin like structure. This conformational change shortens the length between the quantum dot and gold nanoparticle which are attached to the ends of mercury sensitive aptamer. Gold nanoparticles behave as a quenching molecule, and absorb the energy emitted by the quantum dot. This energy transfer, known as fluorescence resonance energy transfer, is a distance dependent phenomenon. Thus, when the distance between the quantum dot and gold nanoparticle shortens, the energy transfer between the two increases. This, subsequently, leads to a decrease in fluorescent intensity – signaling mercury detection.

A DNA linker strand was also conjugated onto the quantum dot. This linker strand contains a pyrene group on its open end. Through $\pi - \pi$ interactions, this linker DNA strand stacks onto graphene oxide causing the molecular beacon to be anchored onto the substrate. Graphene oxide also behaves a quencher, reducing the fluorescent intensity of the quantum dot. To study the degree of quenching graphene oxide has on the system, DNA linker lengths of 14, 35, and 51 base pairs were used to vary the distance between the beacon and the substrate.

It was found at 51 base pairs (~15 nm), the graphene quencher did not hinder the sensitivity of the sensor. At 35 base pairs (~10 nm), the sensitivity slightly decreased, while at 14 base pairs (~5 nm) performance was hampered. All sensors displaced a linear relationship between concentration and quenching efficiency in the nanomolar range. Non-target metal ions were also tested to get an understanding of the specificity of the system, and it was found to have a minuscule effect on the photoluminescence.

I. Background

"There's plenty of room at the bottom" - Richard Feynman

Throughout history, the perception of human progress has been governed on the concept of expanding our frontiers through exploration. First was man's challenge against Mother Nature in his quest to conquer planet earth. Few centuries later, political angst lead to the space race and a man walking on the moon. Modern day, Elon Musk paints a future of a multi-planet civilization. The mainstream view of progress has consistently been "bigger". In the 1980s, advances in instrumentation allowed for the visualization of the world at an atomic level -- opening the door to a new age of scientific discovery.

What makes this atomic level world unique is that is plays by a different set of rules. Classic physics dominates bulk and macroscopic phenomena. Volume, mass, speed can all be measured deterministically. At the nano-scale, $10^{-9}m$, these rules change. A new set of rules- called quantum mechanics governs. This is due to the size of particles of this nature. An example can be illustrated by picturing a spherical particle.

$$Surface\ Area = 4\pi r^2$$

$$Volume = \frac{4\pi r^3}{3}$$

$$\therefore \frac{Surface\ Area}{Volume} = \frac{3}{r} \quad (1)$$

The surface area to volume ratio of a spherical particle is inversely proportional to the radius of the sphere. At the nanoscale, the surface area to volume ratio is uncharacteristically large. A large ratio indicates that most of the atoms, and their valence electrons, are on the surface. Thus, to understand nano-scale interactions, it is critical to understand how these atoms and their electrons behave.

Quantum mechanics can be traced back to the early twentieth century when Max Planck came up with a proportional constant that quantifies the quantum (smallest entity) of light. These entities, later called photons, are quantized (discrete) energy packets. The energy of these packets can be characterized by:

$$E = h * v = \frac{h * c}{\lambda} \quad \therefore E(ev) = \frac{1.24}{\lambda(\mu m)} \ (2)$$

$$h = Plank's\ constant, v = frequency, c = speed\ of\ light, and\ \lambda = wavlength$$

This discovery lead to a big scientific debate on the behavior of light – does it behave as wave or a particle? In 1924, Louis de Broglie extended this theory by hypothesizing that matter can exhibit wave-like characteristics as well. Per his theory, every particle, such as an electron, exhibits behaviors of a particle and wave. Even macroscopic level particles follow this wave-particle duality, but due to their small wavelengths, the phenomena cannot be detected. The wavelength of a particle, called the de Broglie wavelength, can be expressed as:

$$\lambda = \frac{h}{p} \ (3)$$

$$p = momentum$$

When a particle is larger than its de Broglie wavelength, it exhibits bulk like properties such as a continuous energy bands. When the particle is shrunk to the same scale as its de Broglie wavelength, its energy levels become discrete and its band gap starts becoming sized dependent -- a phenomenon known quantum confinement. An illustrative difference between classic and quantum mechanics can be made by comparing the behavior of waves between the two systems.

In classical physics, the one-dimensional wave equation is given as equation 4:

$$\frac{\partial^2\psi}{\partial x^2} \pm \frac{1}{v^2}\frac{\partial^2\psi}{\partial t^2} = 0 \quad (4)$$

$$\therefore \psi(x,t) = \psi(x \pm vt)\ (5)$$

$$\psi = wave\ function\ \ v = velocity\ of\ the\ wave$$

Equation 5 gives the general solution, where the argument represents the phase of the wave. This classical equation is used to describe sound, water, and light waves. However, since in quantum mechanics the goal is to describe the wave nature of a particle, this classical equation becomes obsolete since the equation is not dependent on mass. Erwin Schrödinger solved this problem. Schrödinger's equation is best understood when imaging an electron in an infinite quantum well (potential well).

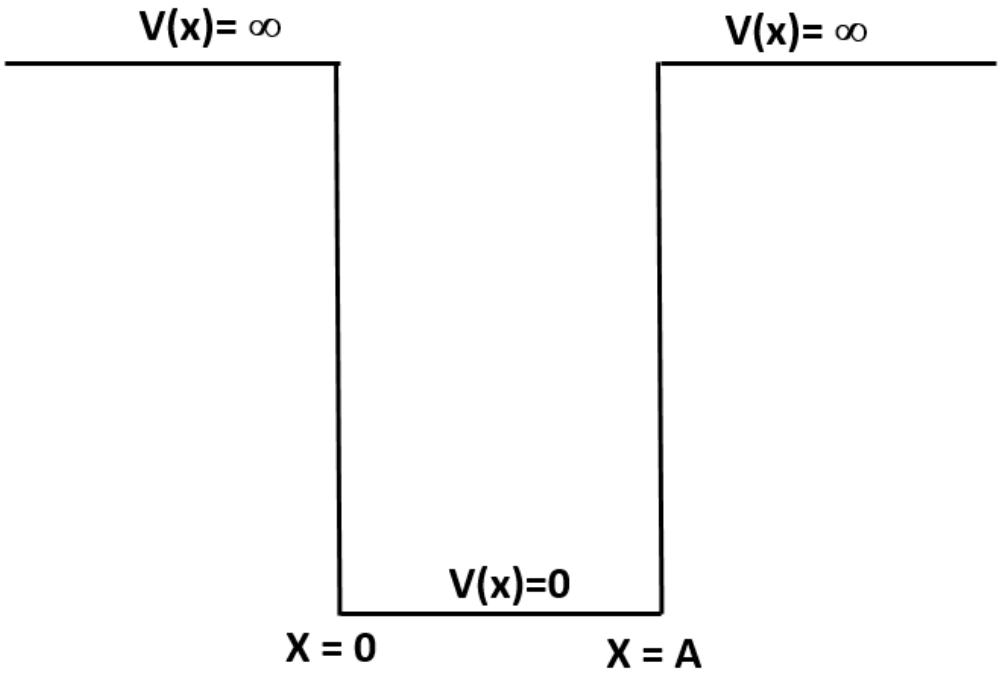

Figure 1: Infinitely Deep Quantum Well, V(x) = ∞ x < 0 and x > A. V(x) = 0 at 0 ≤ x ≤ a.

$$\frac{-\hbar^2}{2m}\frac{d^2}{dx^2}\psi(x) + V(x) = E\psi(x) \quad (6)$$

$$\frac{-\hbar^2}{2m}\frac{d^2}{dx^2}\psi(x) = E\psi(x) \quad (7)$$

$$\frac{d^2}{dx^2}\psi(x) + k^2\psi(x) = \quad (8)$$

$$K.E. = \frac{1}{2}mv^2 = \frac{p^2}{2m}$$

$$E = \frac{h^2}{2m\lambda^2}$$

$$k = \frac{2\,\pi}{\lambda}$$

$$K^2 = \frac{2mE}{\hbar^2}$$

$$\therefore \psi(x) = Bsine(kx) + Ccos(kx) \quad (9)$$

$$\hbar = \frac{Plank's\ constant}{2\pi} \quad m = mass\ of\ the\ particle, V = potential, E = energy$$

$$k = wavenumber$$

Equation 6 represents the one-dimensional Schrödinger's equation. By using the quantum well in Figure 1 and seeing the potential is 0, the jump can be made from equation 6 to 7. Rearranging equation 7 and defining k^2, simplifies the wave function to equation 8. k^2 can be found by taking the classical kinetic energy equation and incorporating the de Broglie wavelength (equation 3). Solving the differential equation gives the general solution in equation 9. Boundary equations are then applied. Since at x = 0, the wave function is 0; the arbitrary constant C must equal 0. Taking equation 10 and applying the second boundary condition, yields equation 11 because k must be a multiple of π to make $\psi = 0$.

$$\psi(0) = 0$$

$$\because \psi(x) = Bsin(kx) \quad (10)$$

$$\psi(a) = 0$$

$$k = \frac{n\pi}{a}; n = 1,2,3,4 \ldots.$$

$$\therefore \psi(x) = Bsin(\frac{nx\pi}{a}) \quad (11)$$

At this juncture, rearranging k allows for the formation of equation 12 which provides the discrete energy value of the quantum system.

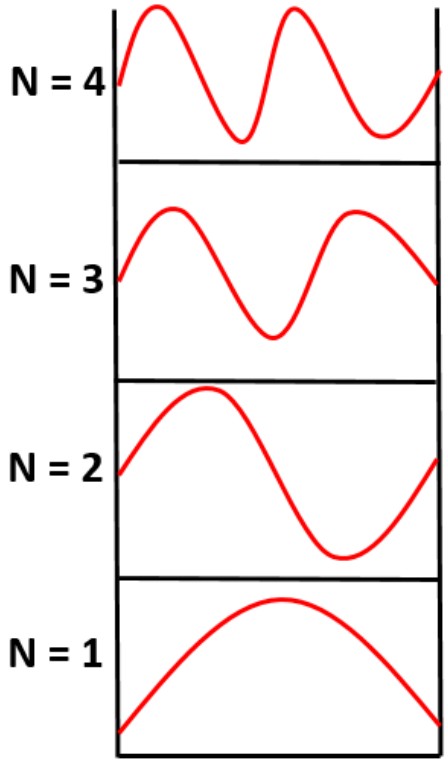

Figure 2: First four energy states in an infinitely deep quantum well.

$$E_n = \frac{\hbar^2 n^2 \pi^2}{2ma^2} \quad (12)$$

By solving through Schrödinger's equation, it is analytically shown why quantum systems have discrete bands of energy. Additionally, by analyzing equation 12, as the size of the quantum well (a) decreases, the energy of the bands increase. This is known as quantum confinement and is used to explain the behavior of quantum dots in the upcoming chapter. Equation 11 needs to be normalized to solve for the constant B.

$$1 = \int_0^a \psi(x)^* \ \psi(x)\, dx$$

$$1 = B^2 \int_0^a sin^2(\frac{nx\pi}{a})\, dx$$

$$B = \sqrt{\frac{2}{a}}$$

$$\psi(x) = \sqrt{\frac{2}{a}} sin\left(\frac{nx\pi}{a}\right) \quad (13)$$

In classical physics, $\psi(x)$ represents the amplitude of the given wave at position x. In quantum mechanics, $\psi(x)$ represents the probability of the electron being at position x. In quantum systems, the location of the electron is never known and only calculated through statistical probabilities. Thus, multiplying $\psi(x)$ by its complex conjugate allows for the normalization of the wave function and the calculation of the arbitrary constant B.

Understanding these quantum systems has allowed engineers and scientists to manipulate matter on the nanoscale to create a field known as nanotechnology. Paralleled with advances in biotechnology, the two fields have intersected to develop technologies that can help human health and environment. This interdisciplinary discipline has allowed for advances in biosensors, drug delivery, diagnostics, medical imaging, tissue engineering, and medical devices [1-4]. The

goal of this research is to illustrate the fabrication, design, and application of a novel biosensor anchored onto a graphene oxide platform for the detection of mercury (II) ions.

II. Nanomaterials

"Great things are done by a series of small things brought together" - Vincent Van Gogh

2.1 Apatmers

Aptamers are single stranded DNA or RNA molecules that have a strong binding affinity towards a preselected target. These targets include -- but are not limited to -- small molecules, metal ions, proteins, and even cells [5]. Deoxyribonucleic Acid (DNA), historically, has been viewed as a genetic carrying biomolecule. Much of the interest in DNA has been focused around its role in the central dogma of molecular biology -- which explains the flow of genetic information. In the early 1990s, an *in vitro* selection technique known as systematic evolution of ligands by exponential enrichment (SELEX) helped produce single stranded oligonucleotides that bind to a desired ligand [6,7]. These oligonucleotide -- referred to as aptamers -- embarked a new area of biochemistry by offering an alternative to antibodies.

A single strand of DNA (ssDNA) is made up of small molecules called nucleotides. Nucleotides consist of a phosphate, sugar, and nitrogenous base. The phosphate and sugar groups give the DNA structure by forming a stable backbone. The final component, the nitrogenous base, carries the genetic code that provides biological instructions. A nucleotide can contain one of four different nitrogenous bases: Adenine (A), Thymine (T), Guanine (G), and Cytosine (C). Each nitrogenous base has a complimentary pair (A-T, G-C) that has a strong affinity toward each other. Two ssDNA with complimentary base pairs form the famously known DNA double helix structure.

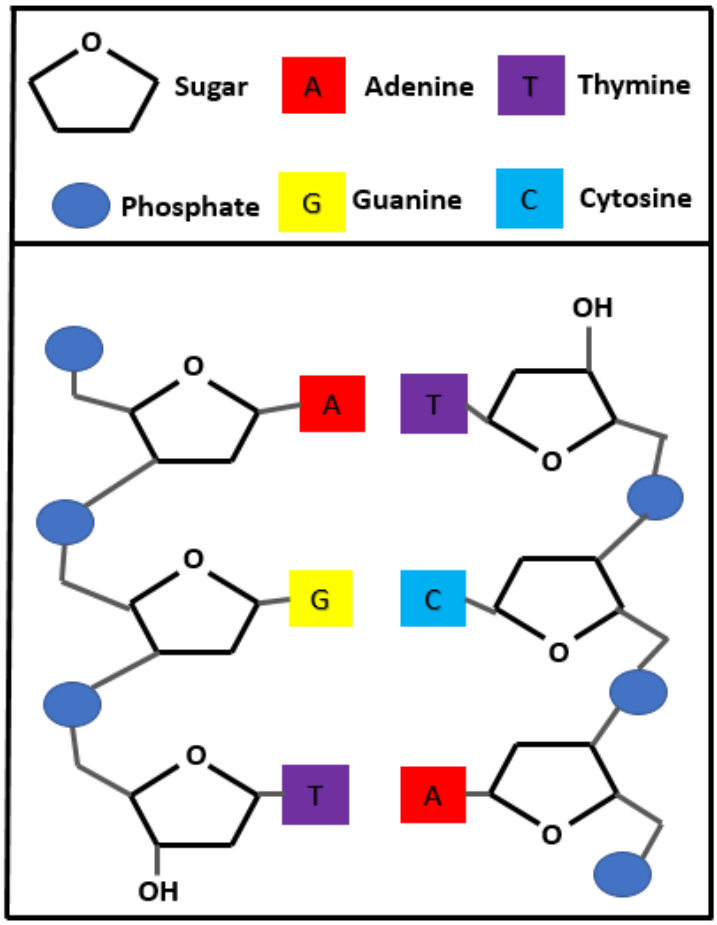

Figure 3: Two complementary ssDNA strands anti-parallel to each other.

SELEX is an *in vitro* chemical process used to determine the aptamer sequence that has strong affinity toward the desired target. The procedure begins with a pool of 10^{14} to 10^{15} randomly unique sequenced oligonucleotides. The DNA in this library have a random region of 20-80 nucleotides, and a constant region of 18-21 bases region at either end [8]. The target is then introduced to the library and binds to certain ssDNA. The ssDNA that shows affinity towards the target -- called aptamers -- are then filtered out. PCR is then performed to amplify the aptamers. The target is reintroduced to these isolated aptamers and this process is repeated until aptamers with strongest affinity are discovered.

Prior to aptamers, antibodies were used as molecular target molecules in many biosensing schemes. Antibodies, also known as immunoglobulin, are large proteins produced by the immune system in the presence of an antigen. In contrast to aptamers, antibodies are produced *in vivo* [9]. When a pathogen such as a virus is introduced, the immune system produces a specific antibody to bind to and offset the antigen. The ability to bind to an antigen gives antibodies the ability to be used as molecular targeting agents. However, antibodies come with disadvantages that aptamers can overcome. The table below compares and contracts the two molecular recognition probes:

Molecular Recognition Probe:	Aptamer	Antibody
Production	In Vitro	In Vivo
Potential Targets	Ions, proteins, cells, small biomolecules	Immunogenic compounds
Chemical Modifications	Straightforward	Limitations

Table 1: Comparison of Aptamers and Antibodies.

2.2 Spherical Nanoparticles

Semiconductor Quantum Dots (QD) are nano-sized spherical semiconductor crystals that contain tunable optical and electrical properties. The ability to control these characteristics makes QDs a useful nanomaterial for engineering done at the nanoscale. Traditionally, organic dyes have been used as fluorescent indicators in many biological and chemical applications. Unfortunately, these dyes have an array of disadvantages including photobleaching and asymmetric emission spectrums [10]. By using QDs, researchers are given a fluorescent indicator that has photostability, tunable emission and broad excitation range, and the ability to conjugate to a

countless number of molecules [11] -- which provides a competitive advantage over organic dyes.

As it stands, QDs are currently being used in a plethora of biosensing, biotagging, and bi-oimaging schemes [12-14]. Their tunable optical characteristics -- to go along with their small sizes -- makes them an ideal candidate for engineered optical nanostructures that sense and detect small molecules such as proteins, cells, and metal ions. A QD can be excited by an incident light, which causes excitation among its electrons. These excited electrons jump from the valence band to the conduction band. During relaxation, the electrons recombine with the electron holes left in the valence band, and during this recombination process energy is released.

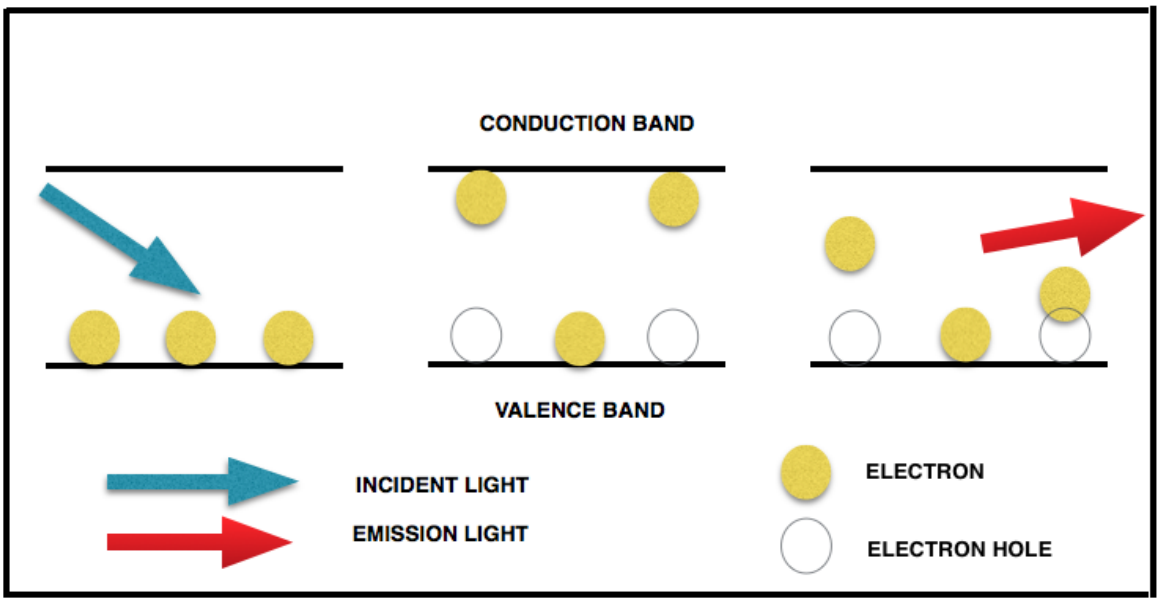

Figure 4: Electron excitation by an indecent light.

The amount of energy released is proportional to the size of the gap between the energy bands. At the nanoscale, these energy bands become discrete and, due to quantum confinement, a decrease in particle size leads to an increase in energy between the discrete energy bands ---

which subsequently results in an increase of released energy. Equation 2 showed that energy released is inversely proportional to the wavelength. Thus, by tuning the size of the QDs, researchers can get a desired optical output.

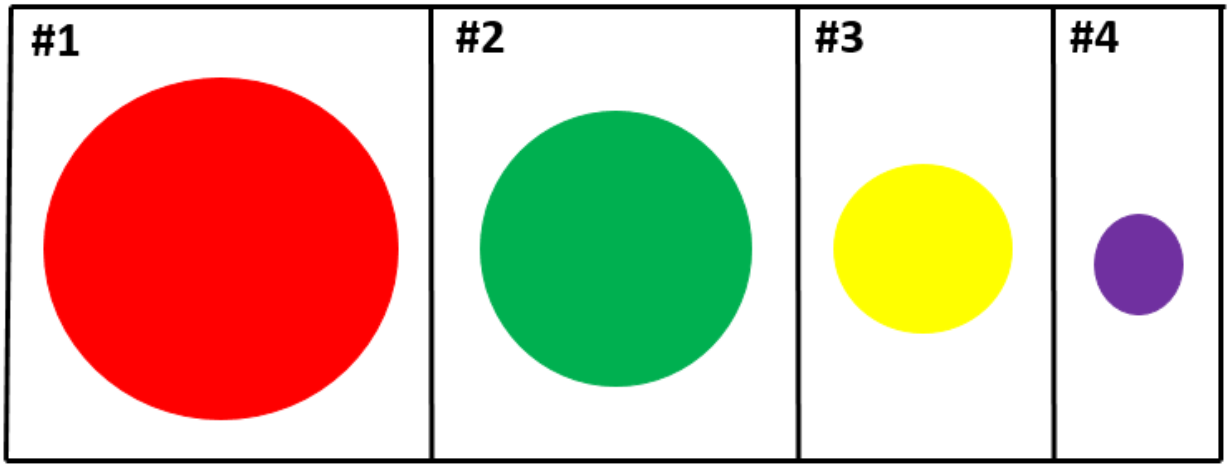

Figure 5: As the size of the QD decreases, the gap between the valence and conduction band increases. This results in an increased amount of energy in the emission light, leading smaller QDs to emit light at a smaller wavelength – thus different colors.

Another unique advantage of QDs is their ability to conjugate to a wide range of molecules through functionalization with a chemical moiety. These functional groups can bind to a desired ligand and later in this work an example of this chemical process is demonstrated.

Gold nanoparticles (AuNPs), also known as colloidal gold, are another group of nanoparticles that has recently gained an increase of research interest. As with quantum dots, AuNPs have tunable optical and electronic properties and have been used in a range of biomedical applications [15-17].

2.3 Graphene and Graphene Oxide

Graphene is a two-dimensional carbon based nanomaterial that has been used for applications in fields ranging from electronics to medicine [18,19]. It has a single atom thick honeycomb structure which provides it with uncharacteristically strong material properties. The covalent bonds between the carbon atoms give graphene extraordinary tensile strength. Graphene's high surface area to volume ratio and strength to weight ratio is starting to get exploited for industrial applications. Carbon nanotubes -- rolled up graphene sheets into a cylinder shape with open ends -- have been used in tennis rackets and hockey sticks to give athletes stronger and lighter sports equipment [20,21]. Additionally, superior electron mobility has provided graphene with applications in nanoelectrons – such as in field effect transistors. The most useful property of graphene, however, might be its ability to be easily modified.

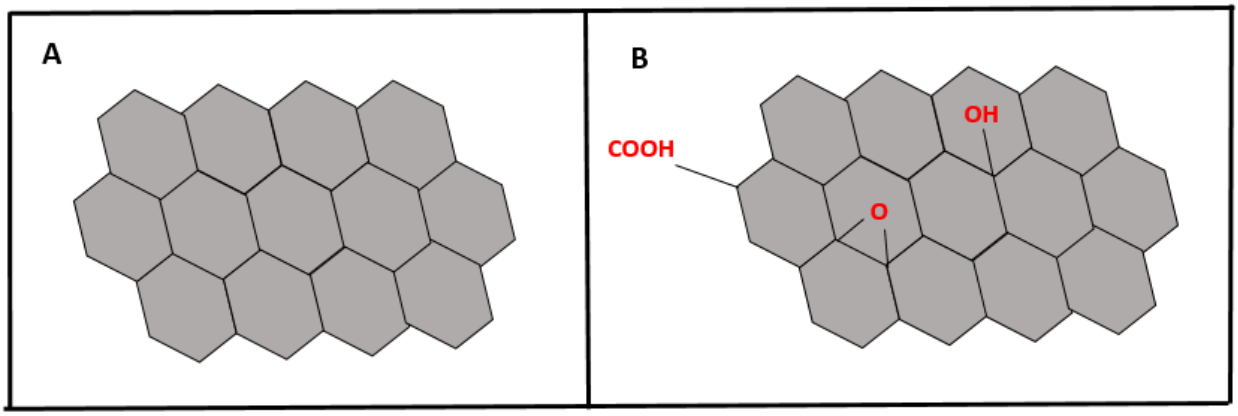

Figure 6: (A) Single sheet of graphene made from carbon atoms. (B) Oxidation of graphene produces oxygen containing functional groups making the product more biocompatible.

Modifying and functionalizing graphene has allowed researchers to expand graphene's applications. Oxidizing graphene gives the material hydroxyl, carboxyl, and epoxy groups while maintaining its carbon-based benzene ring backbone. Oxygen containing functional groups on

graphene oxide (GO) allow for the material to be well dispersed in water. This is of biomedical significance since the human body consists of 55-65% water [22-24]. Additionally, functional groups can be utilized to bind biomolecules or other nanostructures onto the substrate.

III. Energy Transfers

"If you want to find the secrets of the universe, think in terms of energy, frequency, and vibrations" - Nikola Tesla

3.1 Fluorescence Resonant Energy Transfer

Fluorescence Resonant Energy Transfer (FRET) is an energy transfer between an excited donor and a nearby acceptor molecule. This phenomenon is an underlying principle in many optical sensing schemes [25-28]. For FRET to occur, the donor needs to be excited by an incident light. If an acceptor is nearby -- within nanometer -- it may absorb the energy released from the donor. This absorbed energy itself can lead to the excitation of the acceptor which subsequently may lead to emission.

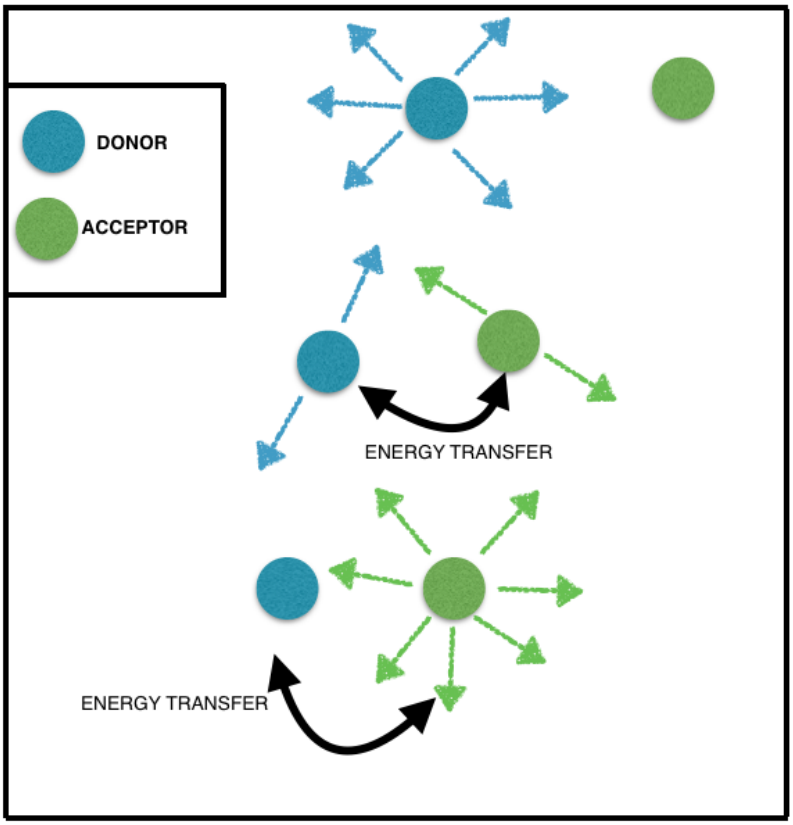

Figure 7: FRET is a distance dependent energy transfer between an excited donor and an acceptor molecule.

The efficiency of the energy transfer between the donor and acceptor is:

$$E_{D-A} = \frac{R_0^6}{R^6 + R_0^6} = \frac{1}{1 + \left(\frac{R}{R_o}\right)^6} \qquad (14)$$

$$E_{D-A} = FRET\ efficiency\ between\ the\ donor\ and\ the\ acceptor$$
$$R = distance\ between\ the\ donor\ and\ acceptor$$
$$R_o = distance\ where\ the\ energy\ transfer\ is\ at\ 50\%$$

As the distance, R, between the donor and acceptor increases, the energy transfer between the two diminishes. R_o can be theoretically calculated by equation 15 [29] :

$$R_o = 0.211[k^2 n^{-4} \emptyset_{QD} J(\lambda)]^{1/6} \quad (15)$$

$$k^2 = dipole\ orientation\ factor$$
$$J(\lambda) = spectral\ overlap\ integral$$
$$\emptyset_D = Quantum\ Yield\ of\ the\ donor$$

The distance between the donor and acceptor can be experimentally calculated by reworking equation 14. This allows for FRET to be used as a spectroscopic ruler to measure the distances between two nanomolecules.

$$\therefore R = R_o * \sqrt[6]{\frac{1}{E_{D-A}} - 1} \quad (16)$$

3.2 Nanometal Surface Energy Transfer (NSET)

Nanometal surface energy transfer (NSET) is another energy transfer between nano-materials with similar mechanisms to that of FRET [30,31]. While the energy transfer during FRET is dipole-dipole, NSET undergoes a dipole-surface transfer between a nanometal surface

and a dipole moment. Like FRET, the transfer between the donor and acceptor is distance dependent. However, an important distinction between the two is the efficiency of the energy transfer.

$$E_{D-A} = \frac{R_0^4}{R^4 + R_0^4} = \frac{1}{1 + \left(\frac{R}{R_o}\right)^4} \quad (17)$$

As seen in equation 17, NSET is more efficient compared to FRET as it is less dependent on the distance between the donor and the acceptor. The size of the acceptor generally determines which energy transfer the system undergoes. An acceptor with a diameter of less than 1.5 nm is expected to undergo a FRET like energy transfer, while if the acceptor is greater than 1.5 nm in diameter, NSET is expected to take over [32,33].

3.3 Quenching

Many biosensors use a phenomenon known as quenching to signal the detection of their target analyte. For quenching to occur, the acceptor must be able to absorb the donor's emission energy. If the acceptor behaves as a quencher, to the naked eye, it appears as the energy of the donor just "disappears". This, however, is not the case due to the first law for thermodynamics stating that energy cannot be created or destroyed. Depending on the acceptor used, thermal energy is released.

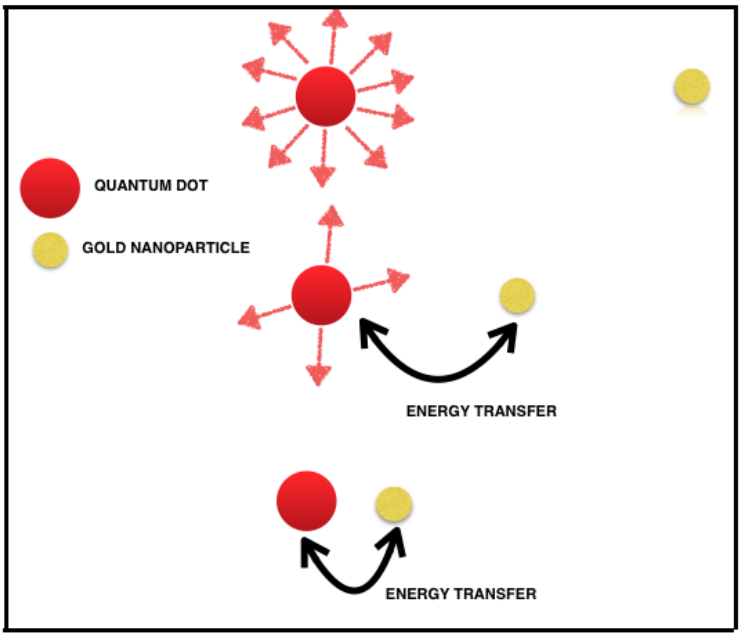

Figure 8: Quenching between an excited Quantum Dot and a Gold Nanoparticle. The Gold Nanoparticle releases thermal energy when excited by the Quantum Dot's emitted photons.

The human eye will not be able to see this emitted thermal energy, so to the viewer only a decrease in the fluorescence of the donor is visible. Since FRET and NSET are distance dependent energy transfers, the closer the quencher is to the fluorescent indicator, the more quenching is observed.

IV. Sensor Design

"Science does not know its debt to imagination" Ralph Waldo Emerson

4.1 Sensor Design

Biosensors have three main elements: the molecular recognition agent, signal producing element, and a transducer. The molecular recognition probe is the bioreceptor molecule that detects the desired analyte. Antibodies and aptamers have both been utilized as molecular recognition probes due to their affinity to desired targets. The signal producing agent provides the signal of the sensor. For optical biosensors, excited fluorescent dyes or quantum dots are used to provide an optical output that can be measured using photoluminescence spectroscopy. Lastly, the transducing element changes the signal of the signal producing molecule upon the presence of the desired analyte. Herein, a mercury target aptamer was used as the molecular recognition agent. 655 Qdots provided the optical signal, and, in the presence of mercury ions, AuNPs transduce the signal provided.

By attaching an aptamer to a QD and an AuNP, the aptamer's conformational change in the presence of the target analyte will change the distance between the two nanoparticles -- resulting in a change in signal. If the distance between the two decreases, the efficiency of the energy transfer increases. Since the gold nanoparticle quenches the energy from the QD, this leads to a decrease in signal. This type of sensor is known as a "turn-off" system because the emission of the system is decreased upon presence of the target.

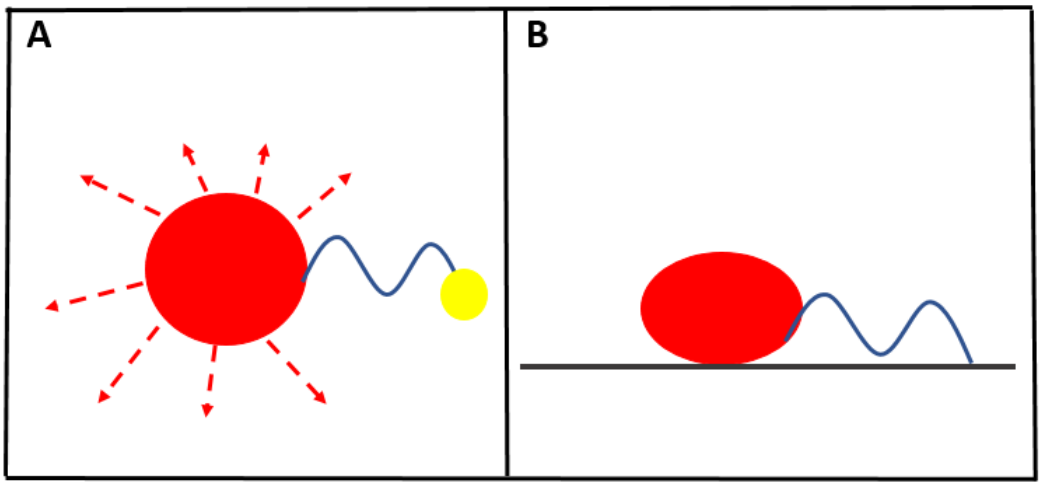

Figure 9: Turn off-sensing system (A) versus a turn-on system (B).

Graphene oxide is commonly used in many "turn on" sensing schemes. By absorbing an aptamer -- QD complex, the GO initially quenches the optical output of the QD. After the addition of the analyte, the aptamer desorbs and the QD's energy can be detected. While molecular beacons have been designed as both "turn off" and "turn on" schemes, to the best of my knowledge, no "turn-off" GO sensor schemes have been demonstrated without labeling the sample with a biomolecule [34,35].

In the present design, a "turn off" molecular beacon is fabricated and then anchored onto a GO substrate. A linker aptamer is used to bind this ensemble onto GO. Since GO is known to be a strong quencher [36,37], different linker lengths were used to study the quenching effect GO has on the molecular beacon. Linker lengths of 51 bps, 35 bps, and 14 bps -- ~ 15 nm, 10 nm, 5 nm in length respectively -- were used.

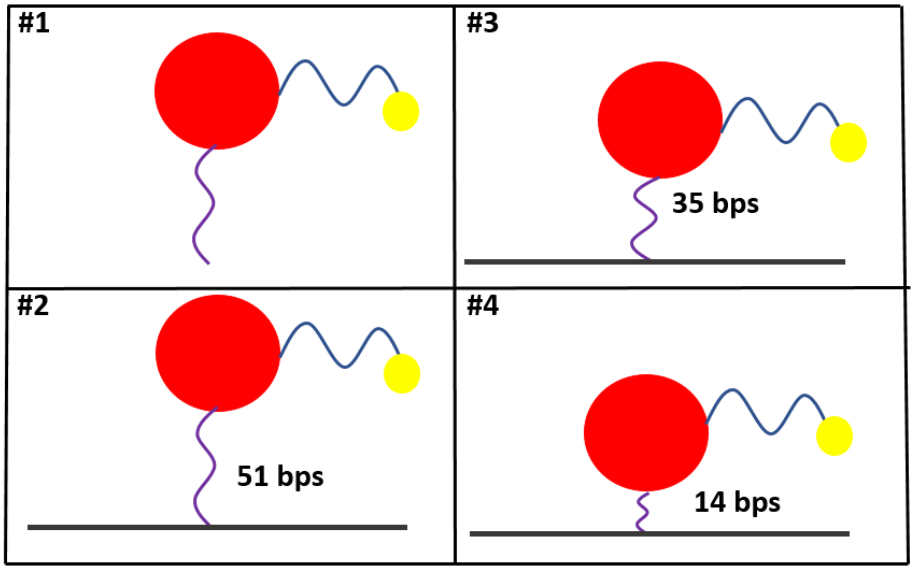

Figure 10: Sensors with linker lengths none, 51 bps, 35 bps, and 14 bps were used to study the quenching effect of graphene oxide.

In the presence of Hg^{2+}, the mercury ions bind to the thymine on the mercury target aptamer [34]. The aptamer undergoes a conformational change, and due to the location of the thymine groups, forms a hairpin structure through Thymine -- Hg^{2+} -- Thymine base pairs [38,39]. This conformational change decreases the distance between the AuNPs (quencher) and the QD (fluorescent indicator). Since the AuNP is less than 1.5 nm in diameter, the interaction between the QD and AuNP is FRET dominated. As the AuNP comes closer to the QD, the transfer efficiency between the two increases and the resulting effect would be a decrease in emission from the 655 Qdot.

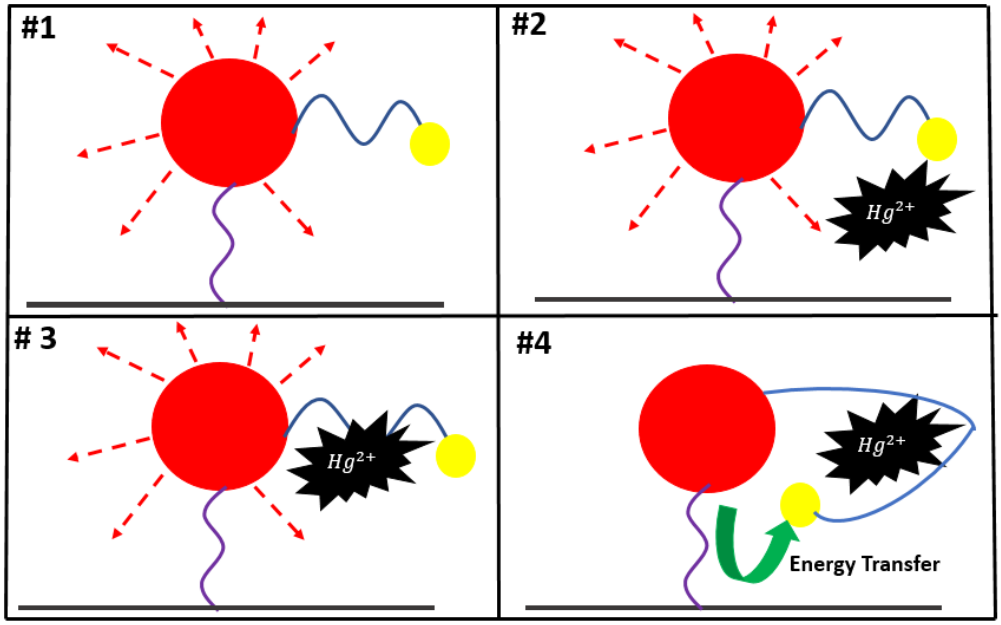

Figure 11: The theory behind the response of the sensor in presence of mercury (II) ions.

Since graphene oxide is also present, quenching between it and the QD may occur. Due to the size of the GO flakes ($0.5\ \mu m\ x\ 0.5\ \mu m$), the energy transfer between the two will is NSET. The efficiency of the energy transfer, however, will be dependent on the linker length.

4.2 Aptamer Selection

Hg^{2+} has a strong affinity toward thymine bases; thus, to create optimal sensitivity in the sensor scheme, a thymine rich aptamer should be chosen to maximize the amount of mercury binding sites. The length of the aptamer is also of importance since FRET is most efficient within 10 nm [40]. Hg^{2+} binds with two thymines forming a Thymine -- Hg^{2+} -- Thymine base pair. By positioning the thymines symmetrically along the aptamer, this enables the formation of a hairpin structure upon the addition of mercury. This conformational change will shorten the distance between a conjugated fluorescent indicator and a quenching acceptor. The sequence 5' d

Amino C6- TTT TTA GGT TGG TGT GGT TGG Thiol C6 SS 3' was chosen, adding functional groups to the ends to allow for binding of nanoparticles.

In determining the sequence for the linker DNA strands, three elements were taken into consideration: 1) Minimizing affinity toward mercury (II) ions 2) Minimizing the possibility of a stem-loop, heterodimer, and homodimer formation and 3) Avoiding the formation of a G-quadruplex. By having a thymine free aptamer sequence, the probability of the aptamer's affinity toward mercury was minimized. To test for potential stem loops, M-Fold Software was used. IDT OligoAnalyzer 3.1 was used to test for heterodimers and homodimers, and QGRS Mapper software was used to predict the possibility of a G-quadruplex formation. All possible dimer formations had a Gibbs Free Energy of around -2.0 kCal/mol -- making it unlikely for formation (~ -9.0 kCal/mol needed). Linkers of 14 base pairs (bps), 35 bps, and 51 bps with a sequence of 5' d Pyrene - dU - $(AG)_x\ A$ -Amino C7 3' were ordered from LGC Biosearch technologies (Novato, CA).

4.3 Nanoparticle Selection

Two critical considerations were taken place during nanoparticle selection: 1) Having appropriate functional groups for bindings purposes and 2) Overlapping emission and absorption spectrum between the donor and the acceptor respectively.

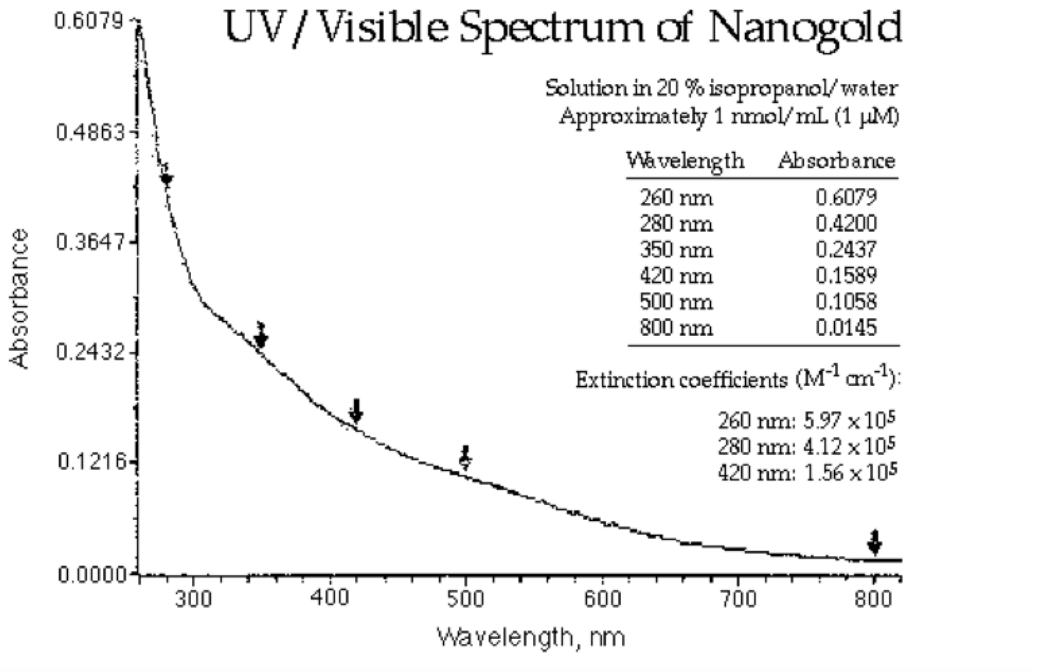

Figure 12: Absorption spectra as given by Nanoprobes (Yaphank, NY, USA).

Qdot® 655 ITK™ carboxyl quantum dots were purchased from Thermo Scientific Fisher Scientific (Waltham, MA, USA). The Qdots have a core made up of CdSe nanocrystals and are coated with a thin layer of ZnS. They are also functionalized with carboxyl groups to allowing for coupling with amine during EDC/Sulfo-NHS chemistry. When excited, the QD releases photons with a peak 655-nm wavelength. The quencher, AuNPs, needs to be able to absorb these photons.

Figure 12 shows that the AuNPs from Nanoprobes (Yaphank, NY, USA) absorbs light covering the entire visible spectrum. Additionally, it emits thermal energy-- making it an ideal candidate to use as a quencher. The AuNPs are coated with a mono-maleimido group to allow for binding. Graphene Oxide flakes ($0.5\ \mu m\ x\ 0.5\ \mu m$) from Graphene Laboratory Incorporated (Calverton, New York, USA) were used.

4.4 Target Analyte

Mercury is a toxic chemical additive that is used in a wide range of industries such as cosmetics and agriculture [41]. Unfortunately, the use of mercury has led to environmental pollution that has caused neurological, reproductive, immunogenic, and carcinogenic effects among humans and other animals [42]. Inorganic mercury, such as mercury (II) ions, can be transformed into the more toxic methylmercury -- the organic form --- through microorganisms that live-in water. Mercury's ability to climb up the food chain creates the necessity to keep the environment mercury free [43]. For example, 80-90% of organic mercury found in the human body is through the consumption of fish and shellfish [44]. Most developed countries have mercury regulations; however, this hasn't prevented contamination in places like Japan, Peru, and the United States of America [45].

To prevent future contamination, improvements in methods of mercury detection need to be made. Current techniques, such as atomic absorption spectroscopy (AAS), Inductively Coupled Plasma Emission Spectroscopy (ICP-ES), and X-ray fluorescence require rigorous training, are expensive, and lack sensitivity [46]. Additionally, they have an inability to provide rapid on-site testing. Biosensors might be able to overcome these limitations, making them an important field of research.

V. Fabrication

"Simplicity is the ultimate sophistication" Leonardo De Vinci

5.1 DNA Preparation

Both mercury sensitive and linker aptamers were dissolved into separate TE buffers (10mM Tris, 1mM EDTA, pH 8.0) to create a 100 µM concentration solution. TE buffer protects the aptamers from degradation and denaturation. Ethylenediaminetetraacetic acid (EDTA) deactivates DNase -- which are enzymes that cleave the phosphodiester linkages. Phosphodiester bonds form when two hydroxyl groups in phosphoric acid react to form two ester groups. These bonds appear on the backbone of DNA strands.

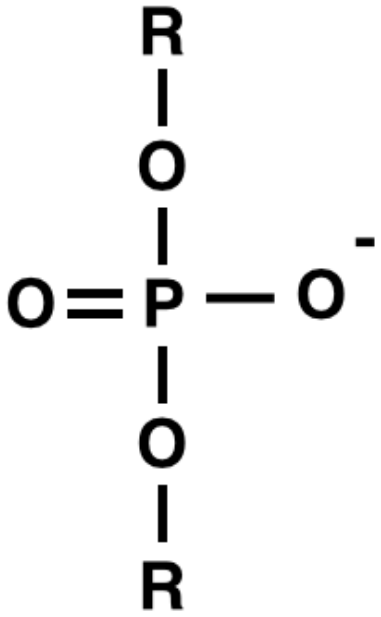

Figure 13: Phosphodiester bond that appears on the backbone of DNA. EDTA deactivates DNase to avoid cleavage of the bond.

5.2 Mercury Aptamer to AuNP

20 μL (2 $nmoles$) of mercury target aptamer was placed into an aliquot. The mercury aptamers were thiol modified to provide a disulfide on the 3' end.

Figure 14: Diagram of thiol modification as provided by DNA Technologies Inc (Coralville, Iowa).

9 μL Tris(2-carboxyethyl) phosphine hydrochloride (TCEP) was used to reduce the disulfide group of the mercury target aptamer. After about 30 minutes of incubation, the disulfide bond is broken. One vial (6 nmols) of mono-maleimido coated AuNP was diluted with 100 μL of deionized water. The diluted AuNPs were then introduced to the aliquot and binding to the reduced groups takes place. AuNPs were introduced in a 3:1 ratio in respect to the mercury target aptamer concentration because the system contains two reduced groups--creating 2 potential binding sites for the AuNP. The aliquot was then incubated at room temperature to allow for the binding to occur.

5.3 Mercury Aptamer – AuNP to Linker and Quantum Dot

After 30 minutes, the Aptamer--AuNP complex was centrifuged at 3,000 RPM. A 3kDalton molecular weight cut off (MWCO) was used to filter out any unbounded material.
9 μL (0.9 $nmols$) of linker aptamer was taken out, to create a 7:3 aptamer to linker ratio on the Qdot. 13 μL (0.1 $nmols$) of Qdot was diluted to 100 μL with a 10-mM borate buffer, pH 7.4. The Qdot and linker DNA were subsequently added to the Aptamer -- AuNP complex. Carbodiimide crosslink chemistry was used to bind the aptamers onto the quantum dot.

As previously mentioned, the Qdots were coated with carboxyl groups. Carboxyls can be activated in the presence of 1-Ethyl-3-(3-dimethylaminopropyl) carbodiimide (EDC). Unfortunately, this creates an unstable o-Acylisourea intermediate that in the presence of water undergoes hydrolysis. To stabilize this product, N-hydroxysulfosuccinimide (Sulfo-NHS) was simultaneously used to create a stable intermediary. This intermediary binds to the amine groups of the functionalized aptamers. 23 μL of 4 $\mu g\ /\mu L$ of EDC/Sulfo NHS (Pierce Biotechnology, Rockford, IL, USA) was introduced to the aliquot. The reaction was kept for 2 hours.

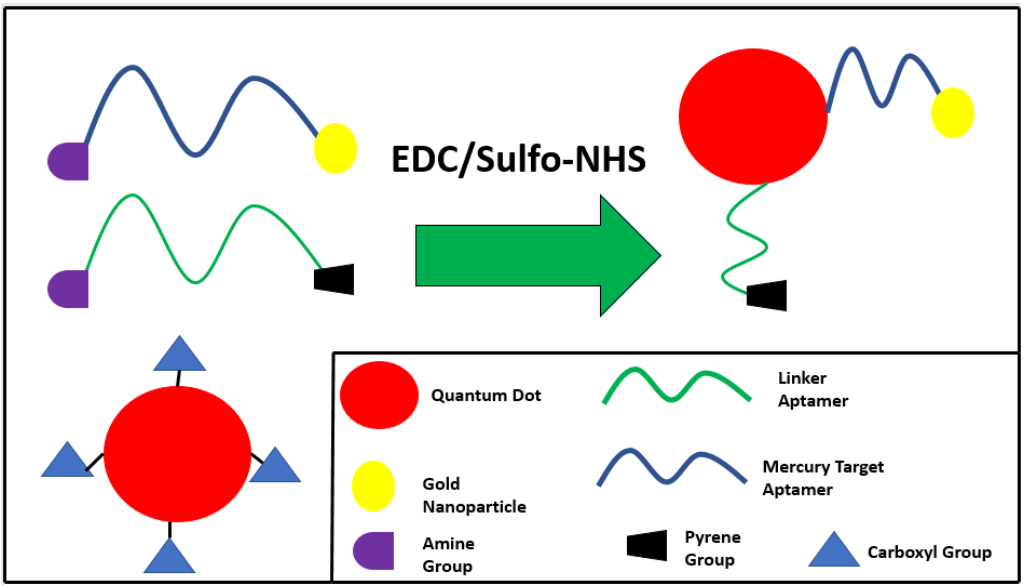

Figure 15: EDC/Sulfo-NHS were introduced simultaneously to avoid hydrolysis.

5.5 Molecular Beacon to Graphene Oxide

The solution was subsequently centrifuged 5 times at 7,000 rpm for 5 minutes in a 100kDalton MWCO and washed with 80 μL of 50-mM borate buffer, pH 8.3. 1 mL of 500 mg/L of graphene oxide (0.5 $\mu m\ x$ 0.5 μm) was added to the beacon assay and incubated overnight to allow for the interaction to take place. The linker aptamer strands have functionalized pyrene groups

on their 5’ end. Pyrene consists of four jointed benzene rings -- like the structure of graphene oxide. Since both the molecular beacon and the GO contain benzene rings, in the presence of one another, a phenomenon known as $\pi - \pi$ stacking occurs. These benzene rings stack on top each other due to attractive non-covalent interactions between pi bonds. After overnight incubation, the solution was equally separated into 4 aliquots and diluted with micropure water to reach 1 mL. Centrifugation at 7,000 rpm was repeated until the resulting supernatant had no visible quantum dots -- indicating disposal of any unbounded Qdots quantum dots.

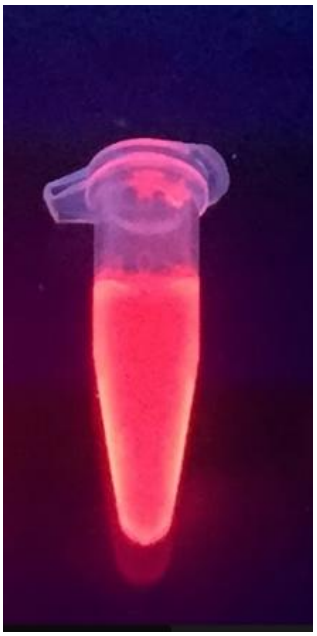

Figure 16: Sensor assay under 365 nm UV light.

VI. Characterization

"There are no shortcuts in evolution" - Louis D. Brandeis

6.1 Photoluminescence spectroscopy

Photoluminescence (PL) is the light emitted from an excited molecule. The intensity of this light can be measured using photoluminescence spectroscopy. In photoluminescence spectroscopy, a liquid assay inside a UV cuvette is placed inside a dark room. A light source excites the assay, causing it to emit photons. The spectrometer then detects the emitted light, and the PL is displayed on the screen.

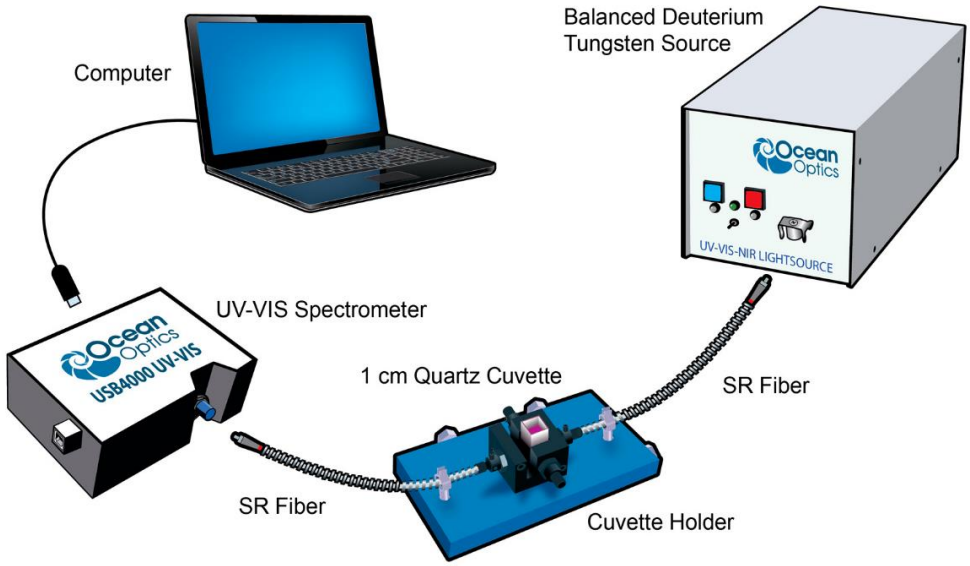

Figure 17: Diagram of Photoluminescence spectroscopy as provided by Ocean Optics (Dunedin, FL).

All photoluminescence measurements were taken using a USB4000 Ocean Optics (Dunedin, FL, USA) spectrophotometer with a continuous LED 375 nm excitation. 750 μL of sensor as-

say was placed inside the cuvette. $HgCl_2$ was dissociated in deionized water to prepare mercury (II) ion samples of different concentrations. Mercury (II) ions were then added into the assay, and the PL and concentration of mercury inside the assay were recorded.

6.2 Data Analysis

In the presence of the sensor, Hg^{2+} ions form a Thymine- Hg^{2+}- Thymine (T-Hg^{2+}-T) complex with the mercury target aptamer. This causes a conformational change in the shape of a hairpin, and since the aptamer is conjugated to AuNPs, there is a decrease in distance between the quencher and the excited QD. Consequently, this leads to decreases of the photoluminescence count.

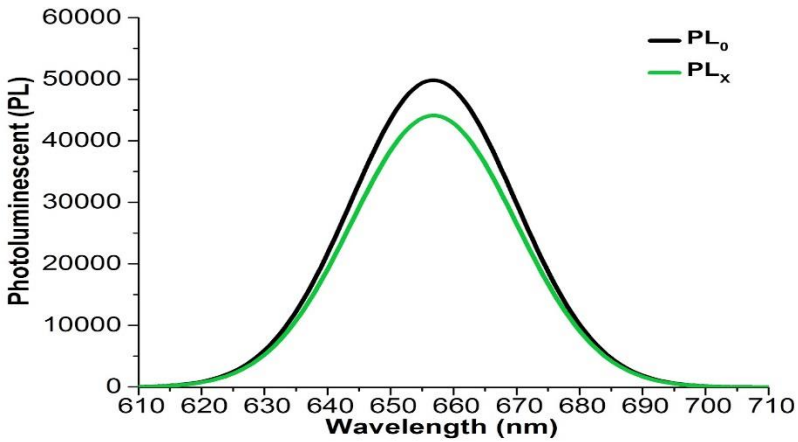

Figure 18: Predicted quenching of the sensor assay.

To normalize between different sensors, percent decrease in photoluminescence was measured. The metric quenching efficiency (QE) was calculated by:

$$QE_x = \frac{(PL_0 - PL_x)}{PL_o} * 100 \quad (17)$$

$$PL_0 = Photoluminescence\ count\ at\ no\ analyte$$

$$PL_x = Photoluminsecence\ count\ at\ concentration\ x$$

QE was calculated over a range of different analyte concentrations. The slope of the calibration curve determines the sensitivity (QE/nM) of the system. The following expression was used to find limit of detection (LOD):

$$LOD = \frac{3 * SD_{PL_o}}{Senstivity} \quad (18)$$

$$SD_{PL_o} = Standard\ deviation\ of\ the\ PL_0\ before\ the\ addition\ of\ analyte$$

VII. Results and Discussion

"If we knew what it was we were doing, it would not be called research, would it?" – Albert Einstein

7.1 Sensor Sensitivity

The sensor's sensitivity is defined as its ability to detect the target analyte. In this study, mercury was added and the calibration curve for each sensor was graphed as seen in Figures 19 and 20. Graphene oxide behaves as a substrate for the molecular beacon and previous studies have illustrated its strong quenching ability [36,37]. This quenching should affect the performance of the sensor, so linkers with varying lengths were used to study the extent.

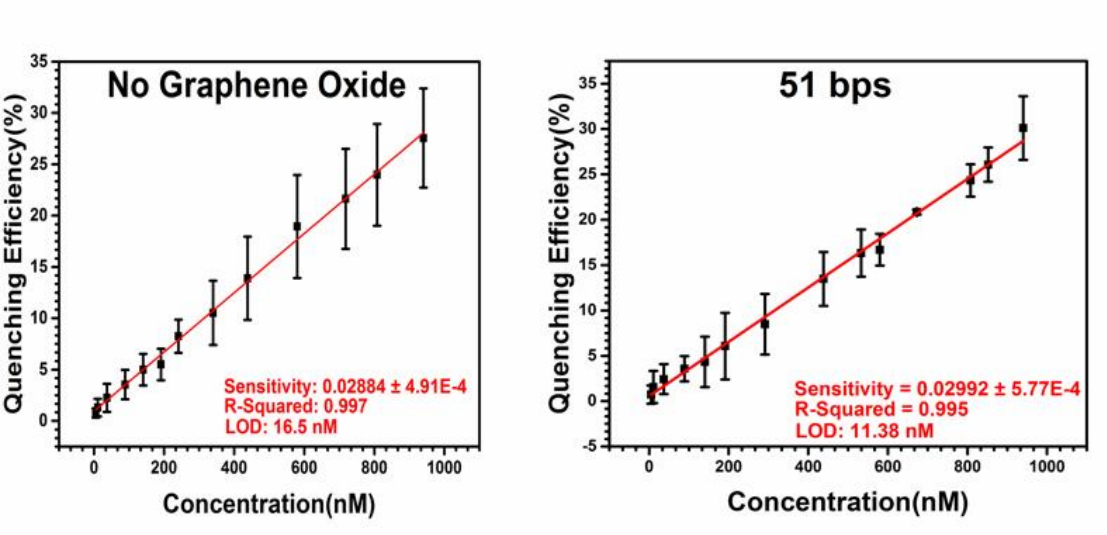

Figure 19: Calibration curve for the no GO (Molecular Beacon) and 51 bps linkers.

Testing was done in the nanomolar range, and all four sensors demonstrated a strong linear relationship ($r^2 > 0.99$) between mercury concentration and QE. The sensitivities of the no (0.02884 ± 4.91E-4) and 51 bps (0.02992 ± 5.77E-4) linkers were within the error range of each other, suggesting at 51 bps (~15 nm) apart, GO does not have a statistically significant quenching ef-

fect on the molecular beacon. The sensor with a 35 bps linker (0.02638 ± 7.89e-4) had a sensitivity slightly lower than the previous two. A 35-bps linker is about 10 nm in length and, at this distance, the results suggest that the quenching effect of GO on the system is minimal at best. However, at 14 bps, the sensitivity (0.02331 ± 3.73E-4) of the sensor significantly decreased. These results suggest that at 14 bps (~ 5nm), graphene oxide has a much higher degree of quenching on the molecular beacon compared to the 35 bps (10 nm) and 51 bps (15nm) linkers. The LOD sensors were found to be 16.5 nM, 38.4 nM, 9.45 nM, and 11.38 nM from no linker to 51 bps linkers respectively.

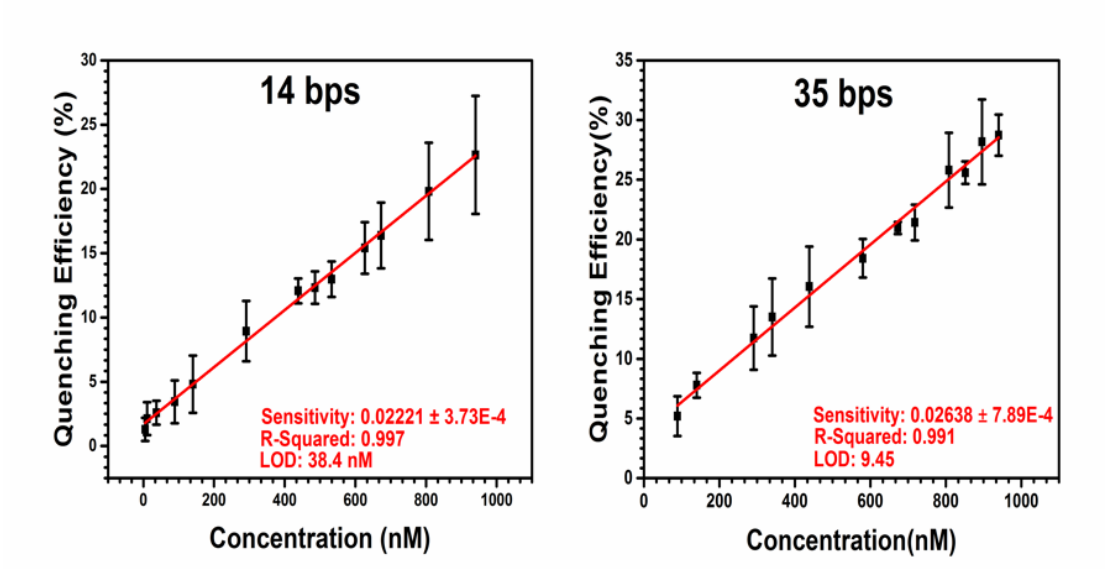

Figure 20: Calibration curves for 14 bps and 35 bps linkers

Two predominate energy transfers are taking place: FRET and NSET. FRET, as modeled by equation 14, takes place between the QD and AuNP. NSET, due to graphene oxide's large surface, happens between the QD and GO and is modeled by equation 17. At 51 bps, the GO and

QD are too far apart for NSET to have an effect of the system. However, at 14 bps, the GO disrupts the energy transfer between the QD and AuNP by creating additional decay paths for the emitted QD energy.

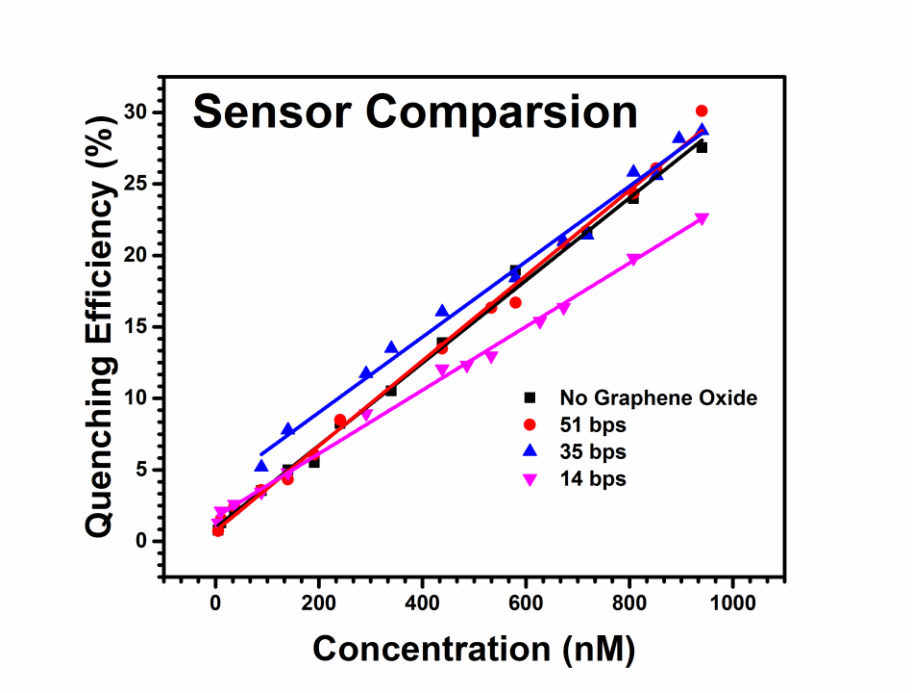

Figure 21: Comparison of all 4 sensors

Since graphene oxide (0.5 μM x 0.5 μM) is much bigger than the AuNPs (1.4 nm), the energy transfer between the QD and GO (NSET) has a dominating effect over the QD – AuNP (FRET) interaction, making the 14 bps system's photoluminescence less dependent on quenching between the AuNP and the QD. Thus, in the presence of mercury, the conformational change bringing the quencher closer to the QD would have a smaller effect on the PL. This results in a decrease in the sensitivity of the sensor as observed.

The Debye Screening Length, named after Peter Debye, measures the length in which a charge separation can occur. By calculating this value, the visibility -- or range of influence -- of

a charged carrier is found. Take a pool of negatively charged particles and positively charged particles (Figure 22).

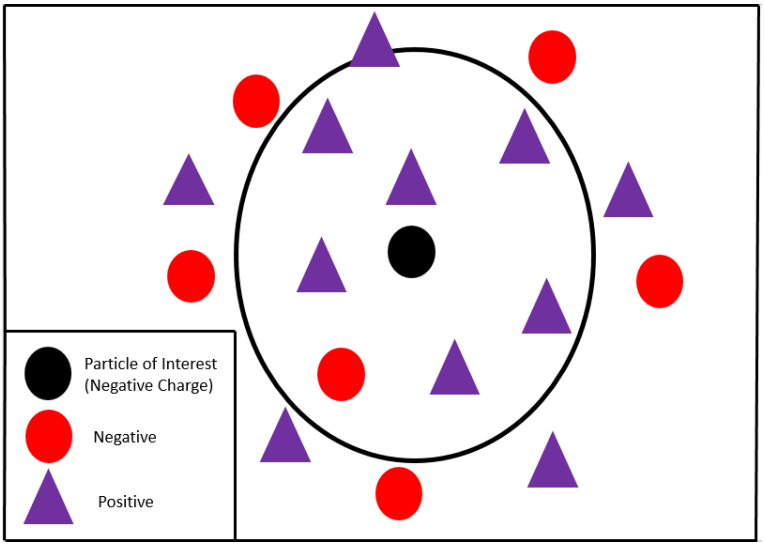

Figure 22: Debye Length of a negative particle.

Opposite charges attract and liked charges repeal, thus the expectation is that the negatively charged particles are shielded from one other and surrounded by positively charged carriers. Therefore, within a certain distance from the negatively charged particles, there will be a surplus of positive charges. This distance represents the Debye Length and is found by the equation below:

$$\lambda_{DL} = \sqrt{\frac{\varepsilon_r \varepsilon_o T \beta}{2 N_a I e^2}} \quad (19)$$

$$I = \frac{1}{2} \sum_{i=1}^{n} c_i {z_i}^2$$

ε_r = dielectric constant of the medium

ε_o = permittivity of free space

$$\beta = \text{Boltzmann constant}$$

$$\text{T} = \text{absolute temperature}$$

$$N_a \text{ is Avogadro's Number}$$

$$\text{e} = \text{ electron charge}$$

$$I = \text{ionic strength of the matrix}$$

$$c_i = molar\ concentration * number\ of\ ions$$

$$z_i = charge\ of\ the\ ion$$

Based on the equation 19, the Debye Length of a charged carrier is inversely dependent on the ionic concentration of the matrix. Aptamers are negatively charged biomolecules, so in the context of an aptasensor, the ionic concentration of the medium effects the sensitivity of the sensor. If an aptasensor is in a matrix consisting of high ionic concentrations, the positively charged non-target ions form a shield around the negatively charged portions of the aptamer [47]. This will decrease the Debye Length of the aptamer, effectively reducing the sensor's ability to "see". The decreased screening length will make it more difficult for the aptamer to bind to the target analyte, lessening the sensitivity of the system. In Figure 23, a 51 bps sensor with a screening length of 1 μm ($no\ ions, pH$ 7.4) was compared with a sensor having a Debye Length of 2.85 nm $\left(ionic\ concentration: 11.34 \frac{mols}{m^3}\right)$.

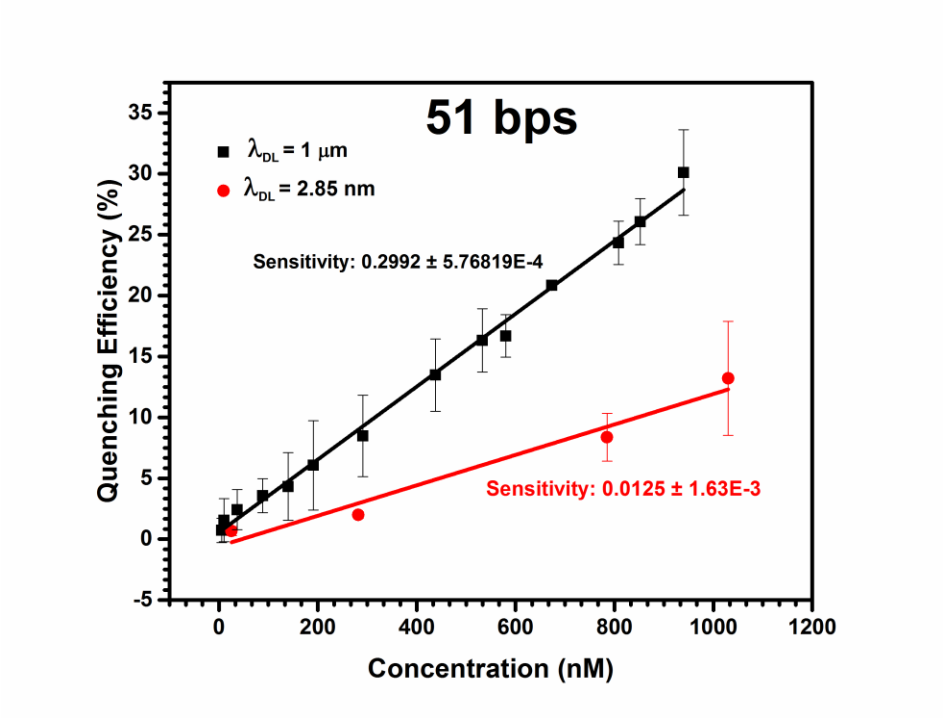

Figure 23: Response of the sensor depending on the Debye Length

7.2 Sensor Specificity

Specificity was defined as the sensor's affinity toward non-target analytes – or the false positive rate. To test the specificity of the system, non-target metal ions: Na^{+}, K^{+}, Zn^{2+}, Li^{2+}, Mg^{2+}, Cd^{2+}, and Co^{2+} where introduce into the assay. High concentrations (>500 μM) of each ion was added. As Figure 24 shows, non-target metal ions had a miniscule effect on the photoluminescence of the system.

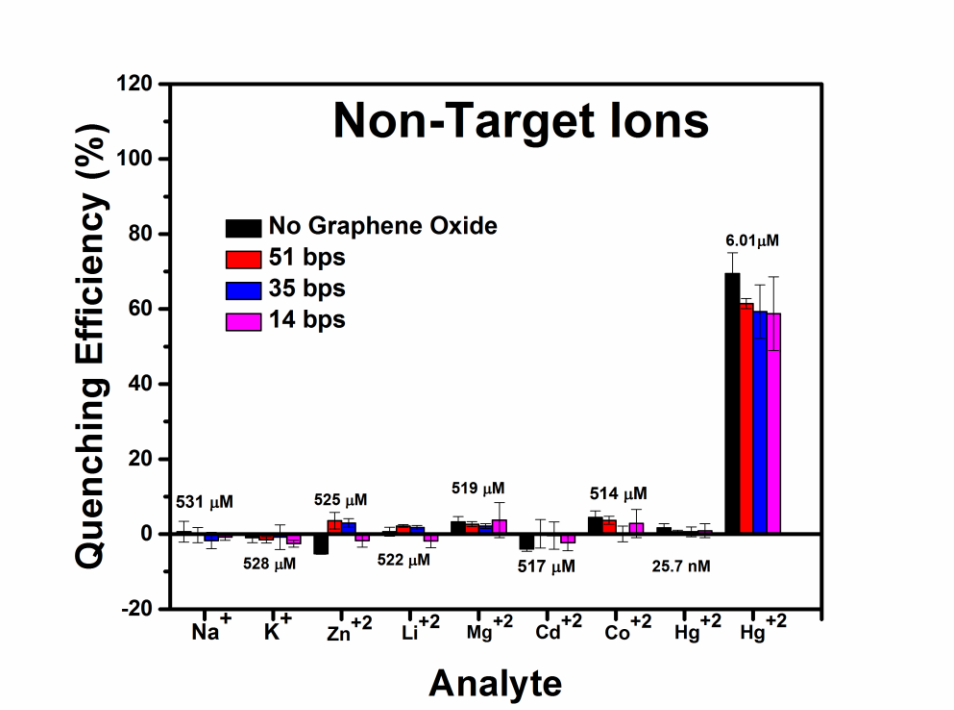

Figure 24: Non-target metal ions

Since the non-target ions were added at such high concentrations, the small change in photoluminescence might not be due to a conformational change in the aptamer. If the aptamer undergoes a conformational change, theoretically, a higher quenching efficiency should be observed. At ~ 500 uM the quenching efficiency of the non-target metal ions were under 10%. In comparison, at 6 uM of mercury, the sensor exhibited about a 60% decrease in photoluminescence. If the non-target metal ions cause a conformational change to the aptamer, the quenching efficiency of a similar magnitude would be observed. Thus, the change of photoluminescence can be potentially attributed to something other than an aptamer conformational change.

Previous studies have shown that DNA loses its persistence length as the salt concentration increases [48,49]. Murphy et al. 2004 suggested that the decrease in persistence length can be attributed to binding of the ions or screening of electrostatic repulsion [46]. As noted earlier, DNA has a phosphodiester bond which contains a free oxygen group on the backbone. This allows the backbone of the DNA to be highly negatively charged – causing electrostatic repulsion between the negative regions of the DNA backbone. These free-floating ions form a shield around these negative regions of the DNA [47]. This shield of positively charged ions causes a screening between the negative regions of the DNA creating an increase in flexibility. This change in flexibility will cause a change in distance between the donor and the acceptor, but is not large enough to create a conformational change – as seen by small change in photoluminescence.

VIII. Conclusion

"You can never plan the future by the past" - Edmund Burke

The results of this work have demonstrated the fabrication, functionality, and working principle of a graphene-oxide based "turn off" sensor. It is shown that anchoring a molecular beacon onto a graphene oxide substrate does not impede the functionality of the sensor at 35 and 51 bps. Additionally, at 14 bps, the sensor's performance was hampered but still displayed functionality. All sensors behaved linearly in the nanomolar range and the sensor displayed low sensitivity toward non-target metal ions -- indicating strong specificity toward mercury.

Graphene oxide has been used for biosensing purposes, but previous studies have shown GO's ability to be used for drug delivery as well. GO's honeycomb like structure allows for the adsorption of other aromatic compounds. In the case of this research, pyrene was functionalized on the 5' end of linker aptamer. This allowed for the adsorption of pyrene through pi staking, which anchored the molecular beacon onto the graphene oxide substrate. Anticancer drugs doxorubicin (DOX) and camptothecin (CPT) contain benzene rings in their molecular structure, and have been shown to adsorb onto GO as a method of controlled loaded [50,51]. Pairing this knowledge with the results presented in this work can potentially lead to theragnostic devices as a method of simultaneously providing detection and therapeutics.

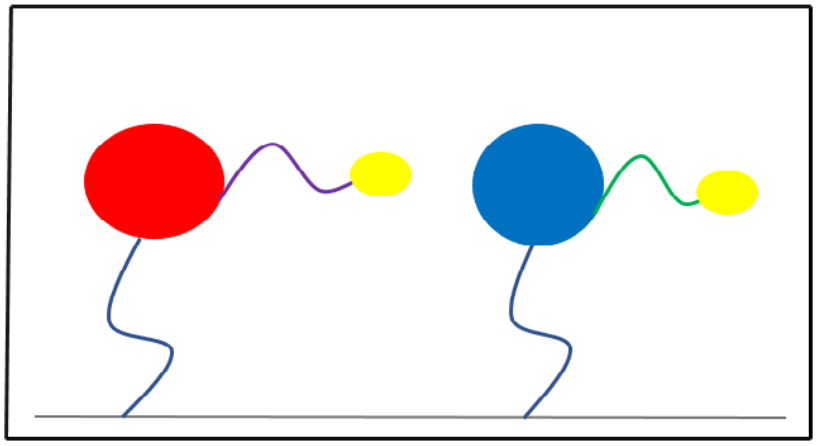

Figure 25: Potential multianalyte detection system on graphene oxide

By replacing the mercury sensitive aptamer with an aptamer of different sensitivity, the system can be expanded for different sensing applications. Additionally, the sensor described herein can potentially be extended to a multiple analyte sensor on the same GO flake by using a variety of different molecular beacons – where different aptamers are paired with different quantum dots that emit light at different wavelengths – on the same GO substrate. This multianalyte device can be beneficial for industrial applications and water testing when multiple poisonous molecules (such as mercury and lead) have potentially contaminated the environment. However, to reach clinical applications, additional specificity testing should be done over a wider range of non-target analytes and further understanding of the mechanism behind false positives needs to be developed.

References

[1] Karunaratne, D. Nedra. "Nanotechnology in medicine." *Journal of the National Science Foundation of Sri Lanka* (2010).

[2] Sepúlveda, Borja, et al. "LSPR-based nanobiosensors." *Nano Today* (2009).

[3] Shi, Jinjun, et al. "Nanotechnology in drug delivery and tissue engineering: from discovery to applications." *Nano letters* (2010).

[4] Baker, Monya. "Nanotechnology imaging probes: smaller and more stable." *Nature Methods* (2010).

[5] Jayasena, Sumedha D. "Aptamers: an emerging class of molecules that rival antibodies in diagnostics." *Clinical chemistry* (1999)

[6] Ellington, Andrew D., and Jack W. Szostak. "In vitro selection of RNA molecules that bind specific ligands." *Nature* (1990)

[7] Tuerk, Craig, and Larry Gold. "Systematic evolution of ligands by exponential enrichment: RNA ligands to bacteriophage T4 DNA polymerase." *Science* (1990)

[8] Stoltenburg, Regina, Christine Reinemann, and Beate Strehlitz. "SELEX—a (r) evolutionary method to generate high-affinity nucleic acid ligands." *Biomolecular engineering* (2007).

[9] Lee, Jeong-O., et al. "Aptamers as molecular recognition elements for electrical nanobiosensors." *Analytical and bioanalytical chemistry* (2008).

[10] Resch-Genger, Ute, et al. "Quantum dots versus organic dyes as fluorescent labels." *Nature methods* (2008).

[11] Frasco, Manuela F., and Nikos Chaniotakis. "Semiconductor quantum dots in chemical sensors and biosensors." *Sensors* (2009).

[12] Yao, Hequan, et al. "Quantum dot/bioluminescence resonance energy transfer based highly sensitive detection of proteases." *Angewandte Chemie International Edition* (2007).

[13] Duan, Hongwei, Min Kuang, and Y. Andrew Wang. "Quantum dots with multivalent and compact polymer coatings for efficient fluorescence resonance energy transfer and self-assembled biotagging." *Chemistry of Materials* (2010).

[14] Gao, Xiaohu, et al. "In vivo cancer targeting and imaging with semiconductor quantum dots." *Nature biotechnology* (2004).

[15] Jeong, Eun Hye, et al. "Gold nanoparticle (AuNP)-based drug delivery and molecular imaging for biomedical applications." *Archives of pharmacal research* (2014).

[16] Kogan, Marcelo J., et al. "Peptides and metallic nanoparticles for biomedical applications." *Nanomedicine* (2007).

[17] Zhang, Xiaoying. "Gold nanoparticles: recent advances in the biomedical applications." *Cell biochemistry and biophysics* (2015).

[18] Zhu, Yanwu, et al. "Graphene and graphene oxide: synthesis, properties, and applications." *Advanced materials* (2010).

[19] Dreyer, Daniel R., et al. "The chemistry of graphene oxide." *Chemical Society Reviews* (2010).

[20] Esawi, Amal MK, and Mahmoud M. Farag. "Carbon nanotube reinforced composites: potential and current challenges." *Materials & design* (2007).

[21] Bierdel, M., et al. "Industrial production of multiwalled carbon nanotubes." *physica status solidi* (2007).

[22] Chang, Yanli, et al. "In vitro toxicity evaluation of graphene oxide on A549 cells." *Toxicology letters* (2011).

[23] Lu, Chun-Hua, et al. "Using graphene to protect DNA from cleavage during cellular delivery." *Chemical Communications* (2010).

[24] Liu, Yong, et al. "Biocompatible graphene oxide-based glucose biosensors." *Langmuir* (2010).

[25] Komatsu, Naoki, et al. "Development of an optimized backbone of FRET biosensors for kinases and GTPases." *Molecular biology of the cell* (2011).

[26] Suzuki, Miho, et al. "Quantum dot FRET biosensors that respond to pH, to proteolytic or nucleolytic cleavage, to DNA synthesis, or to a multiplexing combination." *Journal of the American Chemical Society* (2008).

[27] Aoki, Kazuhiro, et al. "Stable expression of FRET biosensors: a new light in cancer research." *Cancer science* (2012)

[28] Kamioka, Yuji, et al. "Live imaging of protein kinase activities in transgenic mice expressing FRET biosensors." *Cell structure and function* (2012).

[29] Gaudreau, L., et al. "Universal distance-scaling of nonradiative energy transfer to graphene." *Nano letters* (2013).

[30] Jennings, T. L., et al. "NSET molecular beacon analysis of hammerhead RNA substrate binding and catalysis." *Nano letters* (2006).

[31] Griffin, Jelani, and Paresh Chandra Ray. "Gold nanoparticle based NSET for monitoring Mg2+ dependent RNA folding." *The Journal of Physical Chemistry B* (2008).

[32] Ha, Chu Viet, Nguyen Ai Viet, and Tran Hong Nhung. "The local field dependent effect of the critical distance of energy transfer between nanoparticles." *Optics Communications* (2015).

[33] Hoa, N. M., et al. "Simple Model for Gold Nano Particles Concentration Dependence of Resonance Energy Transfer Intensity." *Journal of Physics: Conference Series*. (2016).

[34] Dinda, Diptiman, Bikash Kumar Shaw, and Shyamal Kumar Saha. "Thymine Functionalized Graphene Oxide for Fluorescence "Turn-off-on" Sensing of Hg2+ and I–in Aqueous Medium." *ACS applied materials & interfaces* (2015).

[35] Li, Ming, et al. "Detection of mercury (II) by quantum dot/DNA/gold nanoparticle ensemble based nanosensor via nanometal surface energy transfer." *Analytical chemistry* (2011)

[36] Swathi, R. S., and K. L. Sebastian. "Resonance energy transfer from a dye molecule to graphene." *The Journal of chemical physics* (2008).

[37] Eda, Goki, et al. "Blue photoluminescence from chemically derived graphene oxide." *Advanced Materials* (2010).

[38] Tanaka, Yoshiyuki, et al. "15N− 15N J-coupling across HgII: direct observation of HgII-mediated T− T base pairs in a DNA duplex." *Journal of the American Chemical Society* (2007).

[39] Brenneman, Kimber L., et al. "Aptamer-based optical bionano sensor for mercury (II) ions." *Nanotechnology Materials and Devices Conference (NMDC), (2010.)*

[40] Chen, Huanmian, et al. "Measurement of FRET efficiency and ratio of donor to acceptor concentration in living cells." *Biophysical journal* (2006).

[41] Fernández, J. A., J. R. Aboal, and A. Carballeira. "Use of native and transplanted mosses as complementary techniques for biomonitoring mercury around an industrial facility." *Science of the Total Environment* (2000).

[42] Al-Saleh, Iman, et al. "The extent of mercury (Hg) exposure among Saudi mothers and their respective infants." *Environmental monitoring and assessment* (2015).

[43] Mahaffey, Kathryn R., Robert P. Clickner, and Catherine C. Bodurow. "Blood organic mercury and dietary mercury intake: National Health and Nutrition Examination Survey, 1999 and 2000." *Environmental health perspectives* (2004).

[44] TEACH. Inorganic Mercury, U.S. Environmental Protection Agency, 2007. http://www.epa.gov/teach/chem_summ/mercury_inorg_summary.pdf.

[45] Gochfeld, Michael. "Cases of mercury exposure, bioavailability, and absorption." *Ecotoxicology and Environmental Safety* (2003).

[46] McFarland, Sherri A., and Nathaniel S. Finney. "Fluorescent chemosensors based on conformational restriction of a biaryl fluorophore." *JOURNAL-AMERICAN CHEMICAL SOCIETY* (2001).

[47] Hianik, Tibor, et al. "Influence of ionic strength, pH and aptamer configuration for binding affinity to thrombin." *Bioelectrochemistry* (2007).

[48] Tinland, Bernard, et al. "Persistence length of single-stranded DNA." *Macromolecules* (1997).

[49] Murphy, M. C., et al. "Probing single-stranded DNA conformational flexibility using fluorescence spectroscopy." *Biophysical journal* (2004).

[50] Zhang, Liming, et al. "Functional graphene oxide as a nanocarrier for controlled loading and targeted delivery of mixed anticancer drugs." *Small* (2010).

[51] Liu, Jingquan, Liang Cui, and Dusan Losic. "Graphene and graphene oxide as new nanocarriers for drug delivery applications." *Acta biomaterialia* (2013).

Vita

Arash Derek Darbandi

University of Illinois at Chicago
Masters of Science in Bioengineering, Spring 2017
Thesis: *Graphene Oxide Based Biosensing platform*

University of Illinois at Chicago
Bachelors of Science in Neuroscience, Spring 2014
Honors: *Dean's List, Student-Athlete Academic Honor*

Publications

First Author

Darbandi, A., Datta, D., Krunal, P., Ling, G., Stroscio, M., Dutta, M (2017) "**Molecular Beacon Anchored onto a Graphene Oxide Substrate**" IOP Nanotechnology *(Submitted – currently under review)*

Conferences

Datta, D., **Darbandi, A.**, Stroscio, M., Dutta, M. "**Quantization and Analysis of Acoustic Modes in Rectangular Microsound Nanowaveguide Fixed on a Rigid Substrate**" International Workshop on Computational Nanotechnology June 2017 Windermere, UK *(Abstract accepted)*

Research Experience

Graduate Research Assistant
Nanoengineering Lab January 2016 to Present

- Fabricated aptamer based biosensors
- Performed photoluminescence measurements
- Submitted work to peer review journal, currently under review

Laboratory Assistant
Angiogenesis Lab September 2015 to December 2015

- Assisted in manuscript and grant writing for angiogenesis research

Undergraduate Research Assistant
Biological Microsystems Laboratory August 2013 to July 2014

- Worked under PhD student Elizabeth Ferraz-Samar
- Used NeoFox-GT to measure oxygen concentration in microfluidic devices and silicone and tygon tubing